Green preparation of small-sized starch nanoparticles using nanoprecipitation

Yongxian Chen [a], Li Ding [a], Hongmei Di [b], Jacob Judas Kain Kirkensgaard [c,d], Bekzod Khakimov [c], Bo Sun [b], Chengfang Pang [e,**], Junsheng Chen [f,***], Andreas Blennow [a,*]

[a] Copenhagen Plant Science Center, Department of Plant and Environmental Sciences, Faculty of Science, University of Copenhagen, Denmark
[b] College of Horticulture, Sichuan Agricultural University, Chengdu, 611130, China
[c] Department of Food Science, University of Copenhagen, DK-1958, Frederiksberg C, Denmark
[d] Niels Bohr Institute, Universitetsparken 5, 2100, København Ø, Denmark
[e] Research Group for Genomic Epidemiology, National Food Institute, Technical University of Denmark, Kongens Lyngby, Denmark
[f] Nano-Science Center & Department of Chemistry, University of Copenhagen, Universitetsparken 5, DK-2100, Copenhagen, Denmark

ARTICLE INFO

ABSTRACT

Starch nanoparticles (sNPs) are attractive for numerous applications due to their non-toxicity, environmentally friendly nature, readily available raw materials worldwide, and biodegradability. However, the heterogeneous nature of starch makes it a challenge to prepare homogeneous sNP. The lack of existing preparation methods for small-sized sNPs (ss-sNPs) with high quality has been limiting their practical applications. In this study, we have developed a new method by combining nanoprecipitation and successive centrifugation to generate ss-sNPs with well-defined properties from six different starch types. The method is simple, environmentally friendly, requires a relatively short processing time (<4 h) and generated sizes smaller than 50 nm diameter. The products were thoroughly investigated, structurally, microscopically, and physically. The ss-sNPs products derived from all starch types demonstrated high stability in water (up to three weeks), meeting the requirements for practically any application. The formation of near monodisperse 10 nm diameter ss-sNPs was achieved using a high amylose (more linear) starch type as starting material. However, all ss-sNPs were mainly comprised of short-chained amylopectin. This general and efficient method for producing ss-sNPs offers significant opportunities for their application in various fields.

1. Introduction

Nanoparticles (NPs) provide dimensions ranging from a few nanometers to a few hundred nanometers (in diameter). As compared to bulk materials, NPs possess extreme surface-to-volume ratio, enhanced reactivity, and distinctive optical and electrical properties. NPs have found applications in various fields, including drug delivery (Flores et al., 2019; Mitchell et al., 2021), bioimaging (Erathodiyil & Ying, 2011), catalysis (Astruc, 2020), solar cells (Chen, Seo, Yang, & Prasad, 2013), light emitting diodes (Xing et al., 2016), food (Kou, Faisal, Song, & Blennow, 2023), cosmetics (Arroyo et al., 2020), medicine (Salata, 2004), and agriculture (Zhang, Ying, & Ping, 2022). NPs have hitherto been synthesized using a wide range of chemical materials, such as metals, semiconductors, ceramics, polymers, and organic dyes (Chen et al., 2021; Chen et al., 2023; Chen, Messing, Zheng, & Pullerits, 2019; Khan, Saeed, & Khan, 2019). For biomedical, food, and cosmetic applications, the chemical composition of NPs must provide non-toxic, biodegradable, and environmentally friendly properties. Starch, a bulk natural product derived from our main crops, fulfills all these requirements and is renewable, inexpensive, and readily available worldwide. Consequently, starch-based nanoparticles (ss-sNPs) have attracted increasing attention for critical applications (Corre, Bras, & Dufresne, 2010), such as Pickering emulsions, encapsulation of various agents including pharmaceuticals, nano probes and fat replacer (Caldonazo et al., 2021; Marta et al., 2023).

Apart from the chemical composition of NPs, their applications are also dictated by other physicochemical properties, including size, size

List of abbreviations

AM	Amylose
AP	Amylopectin
ATR-FTIR	Attenuated total reflectance-Fourier transform infrared
CLDs	Chain length distributions
D_2O	Deuterium oxide
DMSO	Dimethyl sulfoxide
DLS	Dynamic light scattering
G50	High amylose content maize starch
^{1}H NMR	Proton nuclear magnetic resonance
NBS	Normal barley starch
NMS	Normal maize starch
NPs	Nanoparticles
NPES	Normal pea starch
NTS	Normal tapioca starch
NWS	Normal wheat starch
WAXS	Wide-angle X-ray scattering
SEC	Size-exclusion chromatography
ss-sNPs	Small-sized starch nanoparticles
TEM	Transmission electron microscopy
TSP	3-(Trimethylsilyl) propionic-2,2,3,3d4 acid sodium salt

distribution, stability, and surface chemistry. Particularly, size and size distribution, i.e., polydispersity, are the most foundational properties of NPs, which play a crucial role in any application. For example, small-sized NPs (<50 nm) are preferred for drug delivery (Villanueva-Flores, Castro-Lugo, Ramirez, & Palomares, 2020), bioimaging (Erathodiyil et al., 2011), and in plant and agriculture (Wang, Lombi, Zhao, & Kopittke, 2016). Specifically, NPs with a size of 40–50 nm exhibit optimal use in terms of uptake and delivery of medical nanodevices (Villanueva-Flores et al., 2020). For specialized use as probes in plant cells, NPs with a size around 10 nm are preferred for efficient penetration of the cell wall, which has a pore size in the range of 5–20 nm (Dietz & Herth, 2011; Eichert & Goldbach, 2008). Moreover, size is a key factor that determines the resolution of bioimaging, and small-sized NPs are preferred for super-resolution bioimaging (Jin et al., 2018). A narrow size distribution is indicative of a well-defined characteristic of NPs, and thus, NPs with a narrow size distribution are attractive for virtually any application.

Different methods have been reported to prepare small-sized (<50 nm, listed in Table S1) sNPs, (ss-sNPs) including strong acid hydrolysis, recrystallization, nanoprecipitation, ultrasonication, gamma irradiation, microemulsion, high-pressure homogenization, and reactive extrusion. However, the prepared ss-sNPs based on these protocols show a rather wide or not even documented size distribution (Table S1). Additionally, very little is known about their hydrocolloidal stability, which is also overlooked in this field (Ahmad, Lim, Navaranjan, Hsu, & Uyama, 2020; Akhavan & Ataeevarjovi, 2012; Bayer et al., 2016; Boufi, Haaj, Magnin, Pignon, & Mortha, 2018; Chao et al., 2016; Dukare, Arputharaj, Bharimalla, Saxena, & Vigneshwaran, 2021; Elham et al., 2015; Gong, Li, Xiong, & Sun, 2016; Haaj, Thielemans, Magnin, & Boufi, 2016; Hasanvand, Fathi, & Bassiri, 2018; Hu et al., 2023; Ip, Tsai, Khimji, Huang, & Liu, 2014; Jiang, Liu, Wang, Xiong, & Sun, 2016; Kheradvar, Nourmohammadi, Tabesh, & Bagheri, 2018; H. Y. Kim, Lee, Kim, Lim, & Lim, 2012; J. Y. Kim & Lim, 2009; Lamanna, Morales, García, & Goyanes, 2013; Maryam, Kasim, Novelina, & Emriadi, 2020; Minakawa, Faria-Tischer, & Mali, 2019; Miskeen, Hong, Choi, & Kim, 2021; Moran et al., 2023; Qin, Liu, Jiang, Xiong, & Sun, 2016; Ruan et al., 2022; Shabana et al., 2018). Apart from these, only strong acid hydrolysis has generated very small size (10 nm) ss-sNPs, and the preparation time is unacceptably long, more than one week (Ayadi et al.,

2016). Phytoglycogen presents as a promising material for the production of small-sized biodegradable NPs, owing to its inherent biodegradability and small particle size. Additionally, high-shear extrusion emerges as a cost-effective and practical technology for the synthesis of small-sized NPs (Roman et al., 2022). Thus, there is a need to develop technology for producing small-sized, narrow size distribution ss-sNPs, conferring high stability in relevant liquid media.

In this work, we report a new protocol combining nanoprecipitation and successive centrifugation, to produce small and well-defined narrow size distributions ss-sNPs. Hence, as compared to previous studies, we focus on obtaining near-monodisperse ss-sNPs using a centrifugation-based separation protocol. We successfully produced ss-sNPs with a size of 10 nm by using this protocol. Followed by the preparation of the ss-sNPs, we analyzed the molecular composition of the prepared ss-sNPs and found their main composition is short-chained amylopectin. This study provides the first simple method for producing ss-sNPs with well-defined size.

2. Materials and methods

2.1. Materials

Normal maize starch (NMS, Commercial Clinton 106) was kindly provided by Archer Daniels Midland (ADM, Decatur, IL, USA). High amylose content maize starch (G50) was purchased from Penford Australia Ltd., NSW, Australia. Normal wheat starch (NWS) was provided by Semper AB (Sweden). Normal barley (NBS) starch was obtained from Svalöf-Weibull AB (Sweden). Normal pea starch (NPES), and normal tapioca starch (NTS) were obtained from KMC (Brande, Denmark).

2.2. Preparation of small-sized starch nanoparticles

Ss-sNP were prepared by a combination of nanoprecipitation and sequential separation process (Fig. 1). Specifically, 2% (w/v) starch (0.8 g) slurry was prepared in MilliQ water (40 mL). Then the mixture was heated up to different temperatures (100 °C for normal starch, 120 °C for high amylose starch) in an oil bath. The temperature was kept for 1 h to ensure a complete gelatinization while keep stirring the mixture at a constant speed (400 RPM). Complete gelatinization was confirmed by iodine staining until there was no starch granule remnants as judged by microscopy. A 4-fold volume of absolute ethanol with 4% (w/v) tween 80 (1.6 mL) was swiftly added in the cooled starch slurry (60 °C). The mixture was stirred at a constant speed (500 RPM) for 1 h followed by centrifugation at 2000g. Finally, the precipitate was collected and redispersed in MilliQ water for further separation of ss-sNPs. In this step, the supernatant was discarded.

In the above-mentioned preparation process, the used parameters were based on previous studies showing ss-sNPs can be prepared at such conditions including the types of starch (normal starch or high amylose starch) (Sadeghi, Daniella, Uzun, & Kokini, 2017), concentration of starch during the nanoprecipitation (Wu et al., 2016), the amount of ethanol as antisolvent for nanoprecipitation (Qiu et al., 2016; Sadeghi et al., 2017). In our study, 4% tween 80 was used to encapsulate the surface of the ss-sNPs, induces the precipitation of ss-sNPs. (Chin, Pang, & Tay, 2011).

At the separation step (Fig. 1), ss-sNPs were obtained using a successive centrifugation process. The centrifugation time of 15 min at different centrifugal speeds (2000g; 4000 g; 6000 g; 8000 g; 10000 g; 15000 g) was used in this experiment. Finally, ss-sNPs were collected in the supernatant after 15,000 g centrifugation.

2.3. Dynamic light scattering (DLS)

The nanoparticle size, size distribution, PDI and zeta potential of ss-sNPs were determined by a Zetasizer (Zetasizer Advance Series - Ultra)
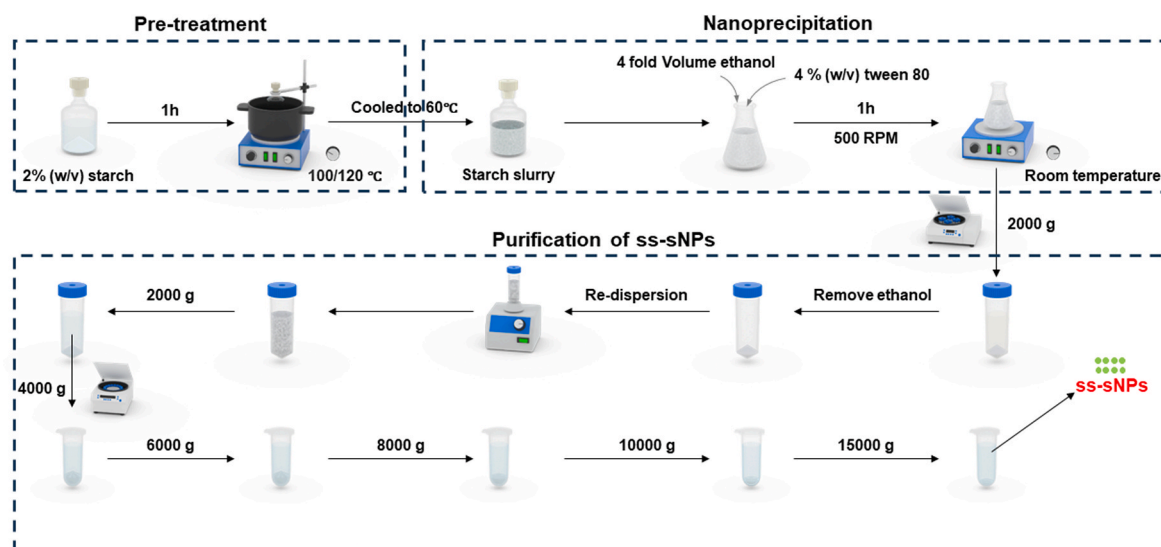
Fig. 1. Schematic illustration for preparation of ss-sNPs combing nanoprecipitation with centrifugation-based separation.

at room temperature. Size, PDI and zeta potential were calculated in triplicate.

2.4. Transmission electron microscopy (TEM)

To visualize the size and morphology of the prepared ss-sNP, we stained them with uranyl acetate as negative stain and the samples were imaged by a Philips CM100 TEM. Statistical analysis of ss-sNP size was conducted based on a minimum of 300 particles from TEM images.

2.5. Determination of the apparent amylose content of native starch and ss-sNPs

Apparent amylose content was estimated by an iodine-affinity protocol as previously described (Zhong, Li, et al., 2021). Five mg of sample in powder form (native starch or ss-sNPs) was dissolved in 0.75 mL of 4 M NaOH with vigorous stirring overnight. The sample was diluted 4-fold with 1 M NaOH and 10 μL solution was added into 200 μL of potassium-iodide (Lugol) solution and absorbance was measured at 620 and 550 nm.

2.6. Size-exclusion chromatography (SEC)

Chain length distributions of debranched samples and analysis of the hydrodynamic radii of the raw samples were monitored by a size exclusion chromatography (SEC)-triple detector array (SEC-TDA) system (Viscotek, Malvern, UK) according to a reported method (K. Wang, Hasjim, Wu, Henry, & Gilbert, 2014). For the preparation of raw sample, 5 mg of sample in powder form was dissolved in 1 mL dimethyl sulfoxide (DMSO, containing 0.55% w/w LiBr). The starch was gelatinized at 80 °C overnight, precipitated and rinsed by 5 mL absolute ethanol twice and the pellet was fully dissolved in 1 mL DMSO (containing 0.55% LiBr) at 80 °C prior to analysis. For analysis of chain length distributions (CLDs) the gelatinized sample was enzymatically debranched with 0.8 U iso-amylase at 40 °C overnight, freeze dried and the debranched powder sample collected. The debranched sample was fully dissolved in 1 mL DMSO (containing 0.55% LiBr) at 80 °C before analysis. For both native and debranched samples, separation was performed in DMSO (0.55% w/w LiBr) at a flow rate of 0.4 mL/min and a column temperature of 60 °C using a SEC instrument equipped with GRAM1000 (Polymer Standard Services, Mainz, Germany) connected to a TDA302 detector array. The differential refractive index (DRI) signals were recorded by a refractive index detector (PN3140, PostNova Analytics, Landsberg,

Germany). Data analysis was carried out by OmniSec Software 4.7 (Malvern Instrument, Ltd, UK). A series of near-monodisperse, pullulan and dextran polysaccharides with molecular weights ranging from 342 to 8.7×10^6 Da were used as external standards. The standards were dissolved in the SEC eluent and then injected into SEC setups to generate universal calibration curves to relate elution volume (Vilaplana, F & Gilbert, 2010).

2.7. Attenuated total reflectance-fourier transform infrared (ATR-FTIR) spectroscopy

The short-range order structure of the native starch granules and ss-sNPs was carried out by a Bomem MB100 FTIR spectrometer (ABB-Bomem, Quebec, Canada) equipped with an attenuated total reflectance (ATR) single reflectance cell with a diamond crystal. The powder samples were scanned 64 times in the spectral range from 600 to 4000 cm^{-1} with a resolution of 8 cm^{-1}, using air as the reference medium. The short-range order was described as the ratio of absorbance between 1047 cm^{-1} and 1022 cm^{-1} based on a previous study (Wang, Wang, Guo, Liu, & Wang, 2017).

2.8. Wide-angle X-ray scattering (WAXS)

The crystalline structures of the samples were carried out by a Nano-inXider instrument (Xenocs SAS, Grenoble, France) equipped with a Cu Kα source with a 1.54 Å wavelength and a two-detector setup according to the method described previously (Zhong, Li et al., 2021). The samples, equilibrated at approximately 90% relative humidity, were enclosed within mica films with a thickness of 5–7 μm before analysis. Samples were scanned through a diffraction angle 2θ range of 5–35° after subtraction from the mica background. The total relative crystallinity was calculated as the ratio between crystalline peak area to the total diffraction area by PeakFit software (Version 4.0, Systat Software Inc., San Jose, CA, USA).

2.9. Proton nuclear magnetic resonance (¹H NMR) spectroscopy

The degree of branching of ss-sNPs were detected by ^{1}H NMR spectra acquired on 600 MHz NMR spectrometer (Bruker Avance III; Bruker Biospin, Rheinstetten, Germany) according to our published protocols (Zhong, Li, et al., 2021). Five mg ss-sNPs were dissolved in 1 mL deuterium oxide (D_2O) and complete gelatinized at 99 °C for 1 h. Afterwards, the gelatinized ss-sNPs were freeze-dried for 24 h. The powder

samples were re-dissolved in 1 mL of a mixture solution containing 900 μL of DMSO with 1.0 mg/mL of 3-(Trimethylsilyl) propionic-2,2,3,3d4 acid sodium salt (TSP) and 100 μL of D_2O. The solubilized starch was heated at 100 °C for 30 min, and 700 μL of the solution was transferred into NMR glass tubes with a length of 178 mm and a diameter of 5.0 mm. The data was acquired using ^1H NMR spectroscopy at a temperature of 60 °C.

2.10. Statistical analysis

All experiments were carried out in triplicates, except for ^1H NMR, which was measured once. Statistical analysis of significant differences (p < 0.05) was performed using Analysis of Variance (ANOVA) followed by Duncan's test with SPSS 25.0 software (SPSS, Inc., Chicago, IL, USA). A time-related trajectory analysis based on a principal component analysis map was performed to visualize temporal changes in stability between different ss-sNP based on two descriptors (size and PDI) using SIMCA-P 14.1 (Umetrics, Umeå, Sweden) (Sun et al., 2021). The correlation results were visualized using Origin 2023b (OriginLab Corporation, Wellesley, MA, USA).

3. Results and discussion

3.1. Preparation of ss-sNPs

As a natural product, starch contains two main components (Fig. 2a): amylose (AM) and amylopectin (AP) (Bertoft, 2017). AM entails a mainly linear structure of α-1,4 linked D-glucose residues and only few branches of α-1,6 linked D-glucose residues. AP is composed of more highly branched structures consisting of shorter chains of α-1,4 linked D-glucose residues and branch-chains of α-1,6 linked D-glucose residues (Fig. 2a). Moreover, the degree of polymerization of each fraction is highly heterogeneous and there is a high genotypic diversity among starches. As a result, during the nanoprecipitation process, both small and large particles can be formed. In the following size characterization, often based on DLS, the presence of large NPs might overshadow the existence of small-sized NPs.

To test this hypothesis and prepare ss-sNPs, we employed a nanoprecipitation method to prepare ss-sNPs and the use of successive centrifugation to separate ss-sNPs from the products (Fig. 1 and Fig. S1). By following the above-mentioned procedure, we choose six different starches as raw materials (Table 1). These starches included normal starches (NMS, NWS, NPES, NTS, NBS) and high-AM starch (G50). Using this nanoprecipitation protocol, we successfully prepared ss-sNPs with hydrodynamic size in the range of 10–30 nm and narrow size distribution (PDI<0.3) (Fig. 2). Among them, ss-sNPs prepared by the G50 starch (termed G50-NP) had the smallest hydrodynamic size of 13 ± 3 nm, which, to our knowledge, is the smallest ss-sNPs reported based on a nanoprecipitation protocol without harsh chemical treatment. The small size of G50-NP was furthermore confirmed by TEM (Fig. 2d) to 10.3 ± 2.2 nm. The size of the other five ss-sNPs were also confirmed by TEM (Figs. S2 and 2f). However, as compared to the DLS data, TEM slightly underestimated the sizes, which can be ascribed to the large hydrodynamic shell around the ss-sNPs (Pabisch, Feichtenschlager, Kickelbick, & Peterlik, 2012) during DLS. The successful preparation of ss-sNP with low PDI based on different starches indicates our method to be widely

Table 1
Preparation of ss-sNPs.

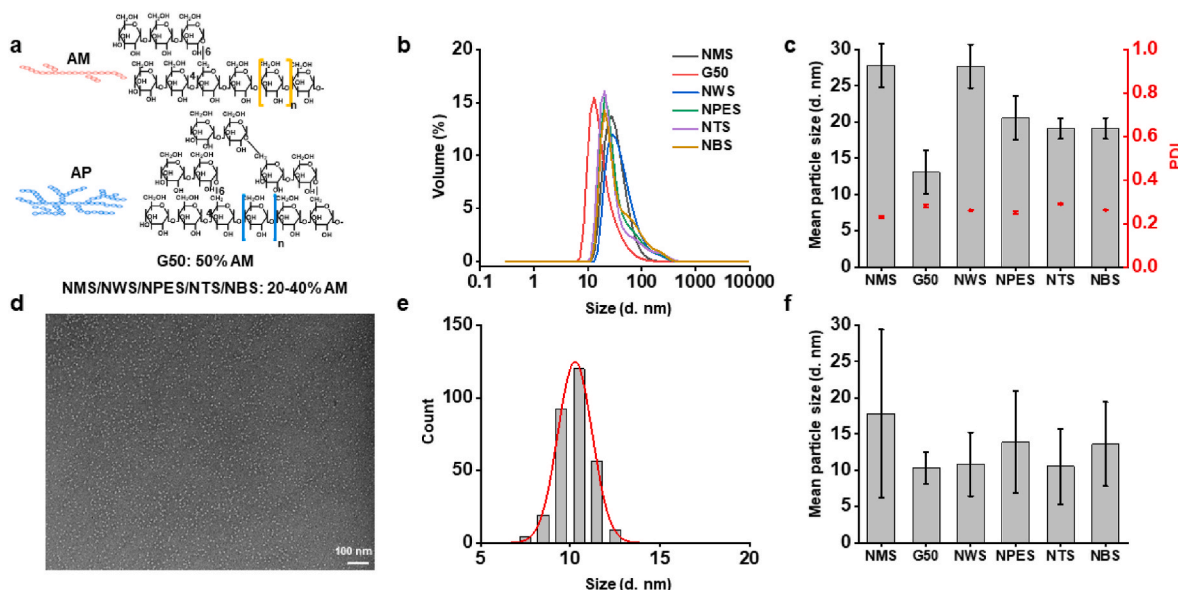| Materials	hydrodynamic size (nm)	Stability	Long-range order (%)
Normal maize starch (NMS): 36% AM	28	More than 7 d	ND
High maize amylose starch (G50): 49% AM	13	More than 21 d	38
Normal wheat starch (NWS): 39% AM	27	More than 21 d	5
Normal pea starch (NPES): 42% AM	21	More than 21 d	ND
Normal tapioca starch (NTS): 23% AM	19	More than 7 d	4
Normal barley starch (NBS): 35% AM	19	More than 21 d	6

ND: not detected.

Fig. 2. The prepared ss-sNPs and size distribution based on different starch a) The structures of six native starches. b-c) The hydrodynamic size distribution (b) and average size (c) of different ss-sNPs acquired from DLS measurements. d-e) TEM image (d) and TEM-based size distributional analysis (e) of size for G50. f) The actual average size of different ss-sNPs. AM, amylose; AP, amylopectin; PDI, polydispersity index; NMS, normal maize starch; G50, high amylose maize starch; NWS, normal wheat starch; NPES, normal pea starch; NTS, normal tapioca starch; NBS, normal barley starch.

applicable. The preparation process only involves common instruments (Fig. 1, hot plate and centrifuge) and environmentally friendly solvents (water and ethanol) and the process takes less than 4 h. The above-mentioned metrics indicate that our method can be widely applied to prepare ss-sNPs in different production sites.

3.2. The composition analysis of ss-sNPs and their formation mechanism

The ss-sNPs formation mechanism is directly linked to the composition of the formed ss-sNPs. Herein, we use G50-NP as a model system to analyze the molecular composition and understand the relevant formation mechanism of the ss-sNPs. Size-exclusion chromatography (SEC) was used to analyze the composition of both G50 native starch and the formed ss-sNP. The composition of the G50 native starch displays two types of starch molecules (AM and AP). These molecular fractions constitute very different chain length distributions (CLDs). With different degree of polymerization (DP) of the constituent chains. Specifically, AP can be divided into chain of DP < 36 and DP 37–100, while AM has considerably longer side chains; DP > 100 (Fig. 3a). After the nanoprecipitation step (Fig. 1), the molecular composition of the suspension (G50-S) was similar to that of the G50 native starch (Fig. 3a). The end-product small-sized G50-NP mainly consisted of AP with low DP side chains, suggesting that these NPs consisted of short chain AP (Fig. 3a). To further confirm the composition of the small-sized G50-NP, we used ^{1}H NMR spectroscopy to analyze the α-1,6:α-1,4 ratios which is

a widely used parameter to determine the degree of branching (composition) of starch materials (Tizzotti, Sweedman, Tang, Schaefer, & Gilbert, 2011). The obtained α-1,6 ratio of the small-sized G50-NP was 13.3, which was much higher than that of waxy maize starch with 100% AP (7.3) (Ding et al., 2023). This result confirms that the composition of G50-NP was mainly short chain AP. The compositional analysis based on SEC revealed that the other five ss-sNPs were also comprised of short chain AP (Fig. 3b) with low molecular weight, which is further supported by the six low apparent AM content of these ss-sNPs (<10%, Fig. 3d) and absolute AM content to be 0% as determined by SEC.

The preparation of ss-sNP involves two phases: i) the nano-precipitation phase (Fig. 1), in which mixed ss-sNPs with different sizes are prepared; ii) the purification phase (Fig. 1), in which ss-sNPs are accumulated via successive centrifugation. Based on the molecular composition and AM contents throughout the preparation process of the small size G50-NP, a possible formation mechanism for the ss-sNPs is suggested (Fig. 3e). The process of preparing ss-sNP involves several important stages. Initially, starch molecules are enclosed within the natural starch granular matrix, supposedly in the form of so called nanoblocklets (Patel, 2018). These undergo complete hydration and gelatinization, and transform into free entities, acting as precursors. During the nanoprecipitation phase, these precursors combine to form ss-sNPs with a wide range of size distribution (e.g., from 10 nm to few μm), hence including a wide distribution of large and small NPs. In the fractionation phase, some AM <textbend>was lost following the
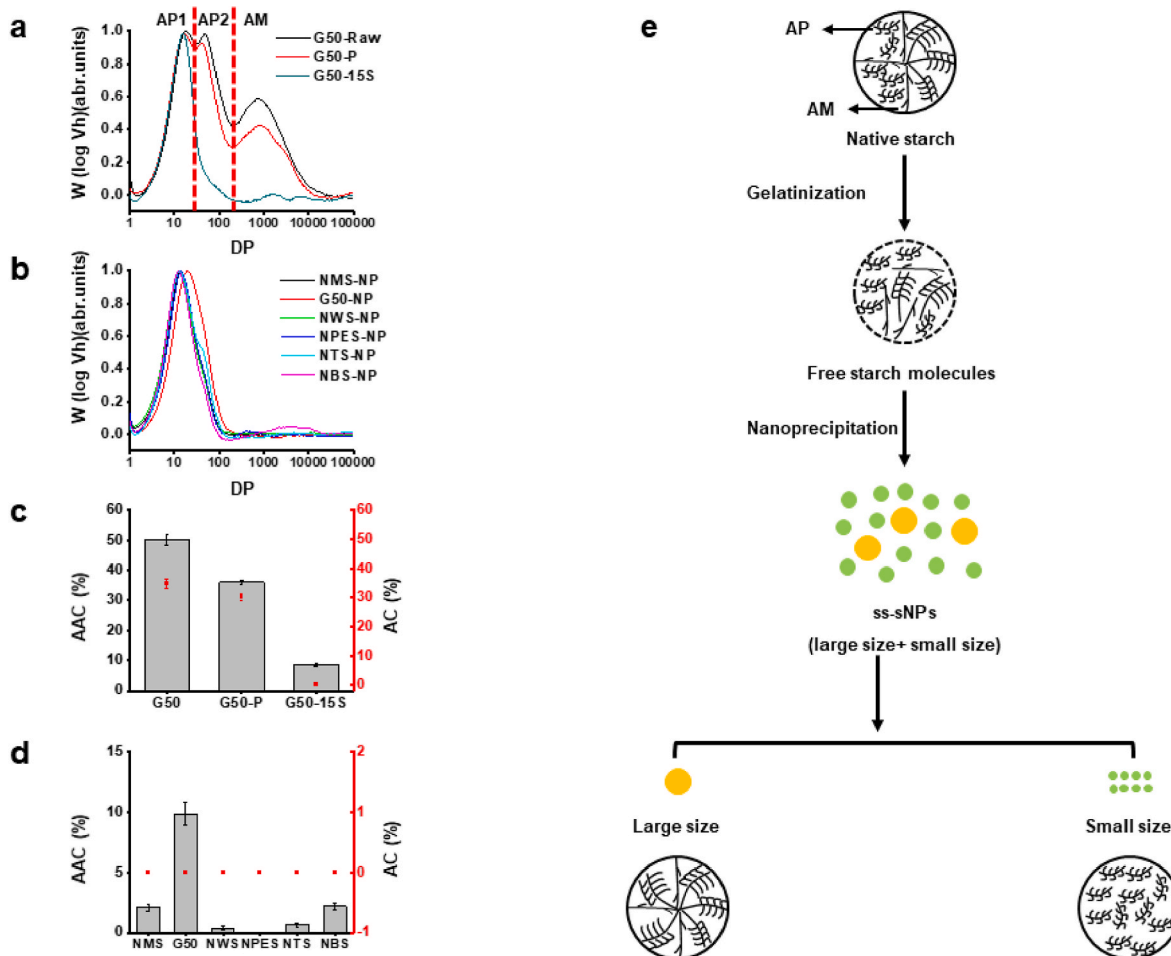

Fig. 3. The possible formation mechanism for ss-sNPs based on composition analysis. a-b) Molecular characteristics of G50-NP from different fractions a) and six different ss-sNPs b). c-d) The apparent and absolute AM content of G50-NP of different fractions c) and ss-sNPs d). e) The proposed formation mechanism of ss-sNPs based on composition analysis. AP1: short AP (DP < 36); AP2: long AP (DP 37–100); AM (DP > 100). G50-Raw: native G50 starch; G50-P: suspension after nanoprecipitation; G50-15 S: G50-NP, supernatant after 15,000 g centrifugation (ss-sNP).

removal of ethanol (Figs. 1 and 3 S4c and S5). Then, centrifugation at a speed of 2000g removed large (micron-sized) particles causing the amount of AM in the supernatant to be higher than in the discarded pellet (Fig. S4c and Fig. S5). This phenomenon arises from the smaller molecular size of AM compared to AP. (Kobayashi, Schwartz, & Lineback, 1985). To separate ss-sNP from the mixture, a series of increasing speed centrifugation steps ranging from 4000 to 15,000 g were employed. This process resulted in the accumulation of AM in the sediment (Figs. S4c and d and Fig. S5) stemming from aggregation of AM with long-chain AP, causing an enrichment of AM in the sediment. Finally, ss-sNPs were acquired from the supernatant after a centrifugal speed of 15,000 g. These ss-sNPs mainly comprised short-chain AP molecules with low molecular weight (Fig. 3b).

3.3. Short-range molecular order and long-range order of ss-sNPs

The short-range molecular order of the prepared ss-sNPs was characterized based on the characteristic bands of the deconvoluted ATR-FTIR spectra. The 800–1200 cm^{-1} range is sensitive to the molecular short-range order of the starch surface, the band around 1047 cm^{-1} is sensitive to the crystalline structure, and the band around 1022 cm^{-1} is related to the amorphous structure (Soest, Tournois, Wit, & Vliegenthart, 1995). Therefore, the ratio between the ATR-FTIR intensity at 1047 cm^{-1} and 1022 cm^{-1} can be applicable to describe the short-range order of starch. Except for G50-NP, the short-range order of all the other ss-sNP were notably lower as compred to the native starch granules (Fig. 4a and Figs. S3a–b). This decrease was expected as an effect of the complete structural destruction of the starch granular crystalline lamellae during gelatinization followed by a non-complete recrystallization of the dissolved material during ss-sNP formation. However, interestingly, for the G50, the short-range order of G50-NP increased significantly as compared to native G50 starch (Fig. 4a and Figs. S3a–b). The significant change in ss-sNP short-range order resulted in a corresponding change in the long-range order of the ss-sNPs. WAXS data showed that only the long-range order of G50-NP increased significantly following the formation of ss-sNPs (Fig. 4b and Figs. S3c–d). Peaks observed at 2θ diffraction angles 21.5° and 23.9° likely resulted from the V-type crystalline pattern from single helix complexing with Tween 80 (Chang, He, & Huang, 2013). Combenedly, the FTIR and WAXS data indicates that native starch with high AM content (G50) has the potential to generate more ordered short- and long-range structures in ss-sNPs.

3.4. Stability of ss-sNPs

The stability in solution of the ss-sNPs was measured based on their change in size and PDI, indicating aggregation, at different time after preparation, and visualized through a time-related principal component trajectory analysis (Fig. 5a and b). The stability of the ss-sNPs is depicted by the distance between its initial coordinate point (the stability data at day 0) and subsequent ones. Hence, close clustering indicates high stability and scattered coordinates suggest low stability. The stability of G50-NP, NPES-NP, and NBS-NP were found higher than those of NWS-NP, NMS-NP, and NTS-NP. G50-NP, NPES-NP, and NBS-NP exhibited stability for at least 21 days (Fig. 5a and b). Although NWS-NP showed a size fluctuation of 7.2 nm within 21 days, its stability remains acceptable due to the manageable size variation (Fig. S6c). NMS-NP becomes unstable after 7 days, with an increase in size from 27.8 nm to 37.6 nm and a PDI from 0.23 to 0.36 at 14 days (Fig. S6a). Despite the increase in PDI from 0.29 to 0.32 for NTS-NP after 7 days, the PDI fluctuation was smaller than that observed for NMS-NP (Fig. S6e). Among the six ss-sNPs, NMS-NP exhibited the lowest stability; nonetheless, its stability is judged suitable for various applications.

The stability of ss-sNPs exhibited a significant correlation with the Zeta-potential of the ss-sNPs, characterized by a strong correlation coefficient of 0.62* (Fig. 5c). This observation aligns with the stability analysis of the six ss-sNPs visualized by PCA. Notably, G50-NP, NPES-NP, and NBS-NP demonstrated higher Zeta-potentials compared to the other three ss-sNPs, which corresponds to their superior stability as indicated by the PCA plot (Fig. 5 and Fig. S7). Additionally, the stability showed a positive correlation (0.67*) with the long-range order of the native starch (LRO-NS) as measured by WAXS relative crystallinity. Furthermore, the variation in PDI showed a higher correlation coefficient (0.53*) with the stability of ss-sNPs compared to the variation in size (0.26) (Fig. 5c). This result indicates that the fluctuation in PDI plays a more significant role in contributing to the stability of ss-sNPs than the fluctuation in average size. The correlation analysis further revealed a robust negative correlation (−0.79*) between the zeta-potential and the AM content of the native starch. This observation can be attributed to the fact that high-AM starch exhibits fewer branched structures compared to normal starch, resulting in a higher degree of exposed regions. The exposed regions may exert an influence on the crystalline structure of starch, consequently impacting its susceptibility to amylase activity and its hydrolytic properties (Lin, Zhao, Li, Guo, & Wei, 2022; Wang, Wang, et al., 2017). Besides, these exposed regions offer more active sites for interactions between starch molecules and surfactants, consequently leading to an augmentation of negative charges on the surface of G50-NP, NPE-NP and NB-NP.

4. Conclusion

In this study, we have reported a simple and environmentally friendly approach, only involving water and ethanol as solvents and nano-precipitants, combining nanoprecipitation and successive
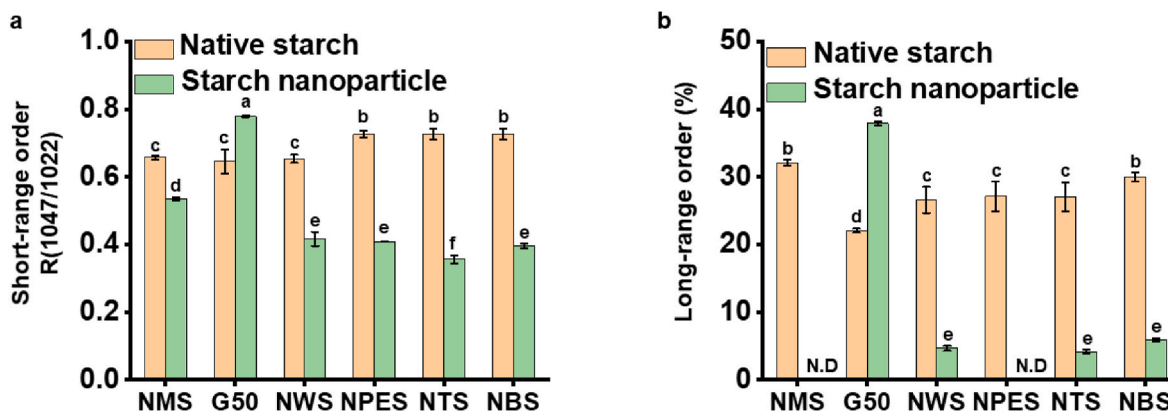

Fig. 4. Short-range molecular order and long-range order of ss-sNPs. a-b) Short-range molecular order a) and long-range order b) of native starch and ss-sNPs detected by ATR-FTIR and WAXS, respectively. ND not detected.
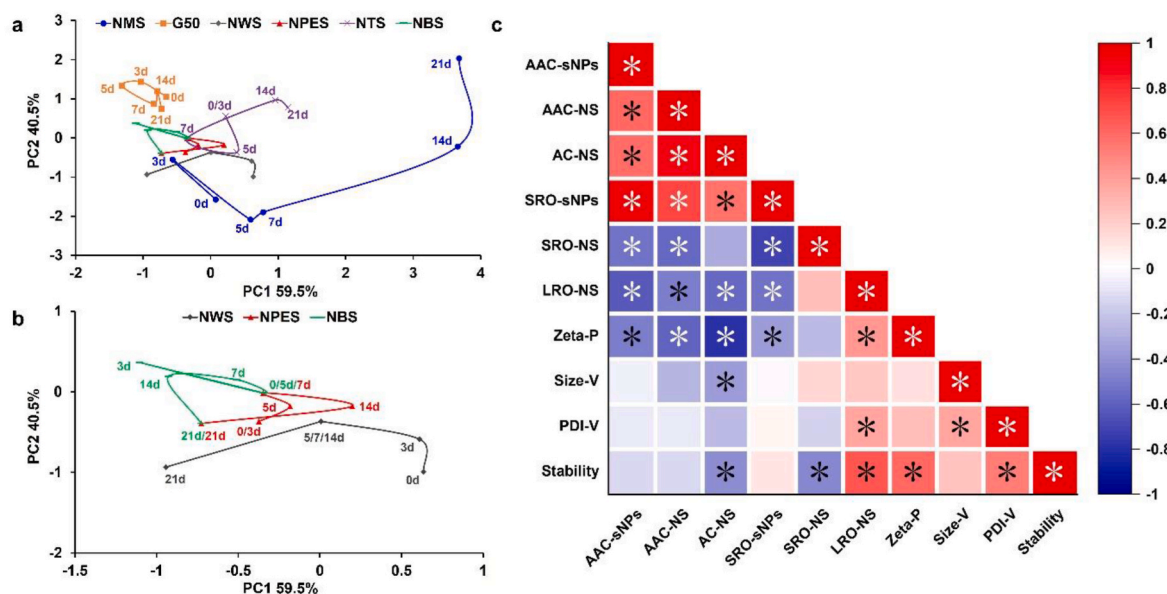
Fig. 5. The stability of different ss-sNPs and correlation plot of correlations between stability of ss-sNPs and other potential factors. a-b) Time-related principal component analysis trajectory plot of stability based on particle size for the six different ss-SNPs. c) Correlation plot of the correlations between stability of ss-sNPs and other potential factors. AAC-ss-sNPs/NS: apparent AM content of ss-sNPs/native starch; AC-NS: absolute AM content of native starch; SRO-ss-sNPs/NS: short-range order of ss-sNPs/native starch; LRO-NS: long-range order of native starch; Zeta-P: zeta-potential; Size-V: the size variations of ss-sNPs; PDI-V: the PDI variations of ss-sNPs; Stability: the stability of ss-sNP.

centrifugation, for producing ss-sNPs. In our approach, we used nano-precipitation to form particles with a broad size distribution, followed with successive centrifugation to separate ss-sNPs with narrow size distributions from the products. By using six different native starches as raw material, we successfully prepared ss-sNPs with hydrodynamic size in the range of 10–30 nm and narrow size distribution (PDI<0.3). The approach is simple, relatively fast (<4 h) and only standard laboratory instrumentation is required. Furthermore, the prepared ss-sNP show high stability up to three weeks for most practical applications. The molecular component analysis reveals that all ss-sNPs are mainly comprised of short-chain amylopectin with content over 90%. Further investigations on the mechanisms behind how a preferably linear (high AM) starting material can be optimal for the generation of a highly branched nanoproduct remains to be done. However, the emphasis on simplicity and universality in our method leads to ss-sNPs with a yield below 10%. We identify two primary approaches by which the yield of ss-sNPs can be enhanced: a) As based on the composition analysis (see section below) the ss-sNPs contains mainly short-chained amylopectin; hence, selecting optimized starch material with short-chained amylopectin as the main composition which can produce a higher fraction of ss-sNPs; b) generating a higher quantity of such starch structures through pre-treatment methods such as ultrasonication.

Our method offers a significant opportunity for using specially engineered starch types as raw material to prepare ss-sNPs with homogeneous size distribution and high stability for different applications. Big and small research groups, regardless of their experience in this field, can be engaged in such ss-sNPs production. This study provides the first simple method for producing ss-sNPs with well-defined size and lays the foundation for the development of ss-sNPs for a wide range of applications.

CRediT authorship contribution statement

Yongxian Chen: Writing – review & editing, Writing – original draft, Visualization, Validation, Supervision, Software, Resources, Project administration, Methodology, Investigation, Funding acquisition, Formal analysis, Data curation, Conceptualization. **Li Ding:** Writing – review & editing, Writing – original draft, Validation, Software,

Methodology, Investigation, Formal analysis, Data curation, Conceptualization. **Hongmei Di:** Writing – review & editing, Writing – original draft, Software, Methodology, Formal analysis, Data curation. **Jacob Judas Kain Kirkensgaard:** Writing – review & editing, Writing – original draft, Validation, Software, Methodology, Formal analysis. **Bekzod Khakimov:** Validation, Software, Methodology, Formal analysis. **Bo Sun:** Writing – review & editing, Writing – original draft, Visualization, Validation, Supervision, Software, Methodology, Investigation, Formal analysis, Data curation, Conceptualization. **Chengfang Pang:** Writing – review & editing, Writing – original draft, Visualization, Validation, Validation, Supervision, Software, Resources, Project administration, Methodology, Investigation, Funding acquisition, Formal analysis, Data curation, Conceptualization. **Junsheng Chen:** Writing – review & editing, Writing – original draft, Visualization, Validation, Supervision, Software, Resources, Project administration, Methodology, Investigation, Funding acquisition, Formal analysis, Data curation, Conceptualization. **Andreas Blennow:** Writing – review & editing, Writing – original draft, Visualization, Validation, Supervision, Software, Resources, Project administration, Methodology, Investigation, Funding acquisition, Formal analysis, Data curation, Conceptualization.

Declaration of competing interest

The authors declare that they have no known competing financial interests or personal relationships that could have appeared to influence the work reported in this paper.

Data availability

Data will be made available on request.

Acknowledgements

(NNF21OC0072082).

Appendix A. Supplementary data

Supplementary data to this article can be found online at https://doi.org/10.1016/j.foodhyd.2024.109974.

References

Ahmad, A. N., Lim, S. A., Navaranjan, N., Hsu, Y. I., & Uyama, H. (2020). Green sago starch nanoparticles as reinforcing material for green composites. *Polymer, 202*, Article 122646.

Akhavan, A., & Ataeevarjovi, E. (2012). The effect of gamma irradiation and surfactants on the size distribution of nanoparticles based on soluble starch. *Radiation Physics and Chemistry, 81*(7), 913–914.

Arroyo, G. V., Madrid, A. T., Gavilanes, A. F., Naranjo, B., Debut, A., Arias, M. T., et al. (2020). Green synthesis of silver nanoparticles for application in cosmetics. *Journal of Environmental Science and Health, 55*(11), 1304–1320. Part Bayer.

Astruc, D. (2020). Introduction: Nanoparticles in catalysis. *Chemical Reviews, 120*(2), 461–463.

Ayadi, F., Bayer, I. S., Marras, S., & Athanassiou, A. (2016). Synthesis of water dispersed nanoparticles from different polysaccharides and their application in drug release. *Carbohydrate Polymers, 136*(20), 282–291.

Bertoft, E. (2017). Understanding starch structure: Recent progress. *Agronomy, 7*(3).

Boufi, S., Haaj, S. B., Magnin, A., Pignon, F., & Mortha, G. (2018). Ultrasonic assisted production of starch nanoparticles: Structural characterization and mechanism of disintegration. *Ultrasonics Sonochemistry, 41*, 327–336.

Caldonazo, A., Almeida, S. L., Bonetti, A. F., Lazo, R. E. L., Mengarda, M., & Murakami, F. S. (2021). Pharmaceutical applications of starch nanoparticles: A scoping review. *International Journal of Biological Macromolecules, 181*, 697–704.

Chang, F., He, X., & Huang, Q. (2013). The physicochemical properties of swelled maize starch granules complexed with lauric acid. *Food Hydrocolloids, 32*(2), 365–372.

Chao, Q., Yang, J., Ge, S., Chang, R., Liu, X., & Sun, Q. (2016). Preparation and characterization of size-controlled starch nanoparticles based on short linear chains from debranched waxy corn starch. *LWT-Food Science & Technology, 74*, 303–310.

Chen, J., Fateminia, S. M. A., Kacenauskaite, L., Baerentsen, N., Gronfeldt Stenspil, S., Bredehoeft, J., et al. (2021). Ultrabright fluorescent organic nanoparticles based on small-molecule ionic isolation lattices. *Angewandte Chemie International Edition in English, 60*(17), 9450–9458.

Chen, J., Kumar, A., Cerretani, C., Vosch, T., Zigmantas, D., & Thyrhaug, E. (2023). Excited-state dynamics in a DNA-stabilized Ag$_{16}$ cluster with near-infrared emission. *Journal of Physical Chemistry Letters, 14*(17), 4078–4083.

Chen, J., Messing, M. E., Zheng, K., & Pullerits, T. (2019). Cation-dependent hot carrier cooling in halide perovskite nanocrystals. *Journal of the American Chemical Society, 141*(8), 3532–3540.

Chen, G., Seo, J., Yang, C., & Prasad, P. N. (2013). Nanochemistry and nanomaterials for photovoltaics. *Chemical Society Reviews, 42*(21), 8304–8338.

Chin, S. F., Pang, S. C., & Tay, S. H. (2011). Size controlled synthesis of starch nanoparticles by a simple nanoprecipitation method. *Carbohydrate Polymers, 86*(4), 1817–1819.

Corre, D. L., Bras, J., & Dufresne, A. (2010). Starch nanoparticles: A review. *Biomacromolecules, 11*, 1139–1153.

Dietz, K. J., & Herth, S. (2011). Plant nanotoxicology. *Trends in Plant Science, 16*(11), 582–589.

Ding, L., Liang, W., Qu, J., Persson, S., Liu, X., Herburger, K., et al. (2023). Effects of natural starch-phosphate monoester content on the multi-scale structures of potato starches. *Carbohydrate Polymers, 310*, Article 120740.

Dukare, A. S., Arputharaj, A., Bharimalla, A. K., Saxena, S., & Vigneshwaran, N. (2021). Nanostarch production by enzymatic hydrolysis of cereal and tuber starches. *Carbohydrate Polymer Technologies and Applications, 2*, Article 100121.

Eichert, T., & Goldbach, H. E. (2008). Equivalent pore radii of hydrophilic foliar uptake routes in stomatous and astomatous leaf surfaces – further evidence for a stomatal pathway. *Physiologia Plantarum, 132*, 491–502.

Elham, H., Milad, F., Alireza, B., Majid, J., Rouzbeh, & Abbaszadeh. (2015). Novel starch based nanocarrier for vitamin D fortification of milk: Production and characterization. *Food and Bioproducts Processing, 96*, 264–277.

Erathodiyil, N., & Ying, J. Y. (2011). Functionalization of Inorganic Nanoparticles for Bioimaging Applications. *Accounts of chemical research, 44*(10), 925–935.

Flores, A. M., Jianqin, Y., Jarr, K.-U., Hosseini-Nassab, N., Smith, B. R., & Leeper, N. J. (2019). Nanoparticle therapy for vascular diseases. *Arteriosclerosis, Thrombosis, and Vascular Biology, 39*(4).

Gong, M., Li, X., Xiong, L., & Sun, Q. (2016). Retrogradation property of starch nanoparticles prepared by pullulanase and recrystallization. *Starch, 68*(3–4), 230–238.

Haaj, S. B., Thielemans, W., Magnin, A., & Boufi, S. (2016). Starch nanocrystals and starch nanoparticles from waxy maize as nanoreinforcement: A comparative study. *Carbohydrate Polymers, 143*(5), 310–317.

Hasanvand, E., Fathi, M., & Bassiri, A. (2018). Production and characterization of vitamin D$_3$ loaded starch nanoparticles: Effect of amylose to amylopectin ratio and sonication parameters. *Journal of Food Science and Technology, 55*(6), 1314–1324.

Hu, W. X., Jiang, F., Ma, C., Wang, J., Lv, X., Yu, X., et al. (2023). Formation mechanism of starch nanocrystals from waxy rice starch and their separation by differential centrifugation. *Food Chemistry, 412*, Article 135536.

Ip, A. C., Tsai, T. H., Khimji, I., Huang, P. J., & Liu, J. (2014). Degradable starch nanoparticle assisted ethanol precipitation of DNA. *Carbohydrate Polymers, 110*, 354–359.

Jiang, S., Liu, C., Wang, X., Xiong, L., & Sun, Q. (2016). Physicochemical properties of starch nanocomposite films enhanced by self-assembled potato starch nanoparticles. *LWT-Food Science & Technology, 69*, 251–257.

Jin, D., Xi, P., Wang, B., Zhang, L., Enderlein, J., & van Oijen, A. M. (2018). Nanoparticles for super-resolution microscopy and single-molecule tracking. *Nature Methods, 15*(6), 415–423.

Khan, I., Saeed, K., & Khan, I. (2019). Nanoparticles: Properties, applications and toxicities. *Arabian Journal of Chemistry, 12*(7), 908–931.

Kheradvar, S. A., Nourmohammadi, J., Tabesh, H., & Bagheri, B. (2018). Starch nanoparticle as a vitamin E-TPGS carrier loaded in silk fibroin-poly(vinyl alcohol)-Aloe vera nanofibrous dressing. *Colloids and Surfaces B: Biointerfaces, 166*, 9–16.

Kim, H. Y., Lee, J. H., Kim, J. Y., Lim, W. J., & Lim, S. T. (2012). Characterization of nanoparticles prepared by acid hydrolysis of various starches. *Starch, 64*(5), 367–373.

Kim, J. Y., & Lim, S. T. (2009). Preparation of nano-sized starch particles by complex formation with n-butanol. *Carbohydrate Polymers, 76*(1), 110–116.

Kobayashi, S., Schwartz, S. J., & Lineback, D. R. (1985). Rapid analysis of starch, amylose and amylopectin by high-performance size-exclusion chromatography. *Jounrnal of Chromatography A, 319*, 205–214.

Kou, T., Faisal, M., Song, J., & Blennow, A. (2023). Stabilization of emulsions by high-amylose-based 3D nanosystem. *Food Hydrocolloids, 135*, Article 108171.

Lamanna, M., Morales, N. J., García, N. L., & Goyanes, S. (2013). Development and characterization of starch nanoparticles by gamma radiation: Potential application as starch matrix filler. *Carbohydrate Polymers, 97*(1), 90–97.

Lin, L., Zhao, S., Li, E., Guo, D., & Wei, C. (2022). Structural properties of starch from single kernel of high-amylose maize. *Food Hydrocolloids, 124*, Article 107349.

Marta, H., Rizki, D. I., Mardawati, E., Djali, M., Mohammad, M., & Cahyana, Y. (2023). Starch nanoparticles: Preparation, properties and applications. *Polymers, 15*(5).

Maryam, Kasim, A., Novelina, & Emriadi. (2020). Preparation and characterization of sago (*metroxylon* sp.) Starch nanoparticles using hydrolysis-precipitation method. *Journal of Physics: Conference Series, 1481*, Article 012021.

Minakawa, A. F. K., Faria-Tischer, P. C. S., & Mali, S. (2019). Simple ultrasound method to obtain starch micro- and nanoparticles from cassava, corn and yam starches. *Food Chemistry, 283*(15), 11–18.

Miskeen, S., Hong, J. S., Choi, H. D., & Kim, J. Y. (2021). Fabrication of citric acid-modified starch nanoparticles to improve their thermal stability and hydrophobicity. *Carbohydrate Polymers, 253*(4), Article 117242.

Mitchell, M. J., Billingsley, M. M., Haley, R. M., Wechsler, M. E., Peppas, N. A., & Langer, R. (2021). Engineering precision nanoparticles for drug delivery. *Nature Reviews Drug Discovery, 20*(2), 101–124.

Moran, D., Gutierrez, G., Mendoza, R., Rayner, M., Blanco-Lopez, C., & Matos, M. (2023). Synthesis of controlled-size starch nanoparticles and superparamagnetic starch nanocomposites by microemulsion method. *Carbohydrate Polymers, 299*, Article 120223.

Pabisch, S., Feichtenschlager, B., Kickelbick, G., & Peterlik, H. (2012). Effect of interparticle interactions on size determination of zirconia and silica based systems – a comparison of SAXS, DLS, BET, XRD and TEM. *Chemical Physics Letters, 521*(C), 91–97.

Patel, A. R. (2018). Functional and engineered colloids from edible materials for emerging applications in designing the food of the future. *Advanced Functional Materials, 30*(18).

Qin, Y., Liu, C., Jiang, S., Xiong, L., & Sun, Q. (2016). Characterization of starch nanoparticles prepared by nanoprecipitation: Influence of amylose content and starch type. *Industrial Crops & Products, 87*, 182–190.

Qiu, C., Yang, J., Ge, S., Chang, R., Xiong, L., & Sun, Q. (2016). Preparation and characterization of size-controlled starch nanoparticles based on short linear chains from debranched waxy corn starch. *LWT-Food Science & Technology, 74*, 303–310.

Roman, L., Baylis, B., Klinger, K., Jong, J. D., Dutcher, J. R., & Martinez, M. M. (2022). Changes to fine structure, size and mechanical modulus of phytoglycogen nanoparticles subjected to high-shear extrusion. *Carbohydrate Polymers, 298*, Article 120080.

Ruan, S., Tang, J., Qin, Y., Wang, J., Yan, T., Zhou, J., et al. (2022). Mechanical force-induced dispersion of starch nanoparticles and nanoemulsion: Size control, dispersion behaviour, and emulsified stability. *Carbohydrate Polymers, 275*, Article 118711.

Sadeghi, R., Daniella, Z., Uzun, S., & Kokini, J. (2017). Effects of starch composition and type of non-solvent on the formation of starch nanoparticles and improvement of curcumin stability in aqueous media. *Journal of Cereal Science, 76*, 122–130.

Salata, O. V. (2004). Applications of nanoparticles in biology and medicine. *Journal of Nanobiotechnology, 2*(1), 3.

Shabana, S., Prasansha, R., Kalinina, I., Potoroko, I., Bagale, U., & Shirish, S. H. (2018). Ultrasound assisted acid hydrolyzed structure modification and loading of antioxidants on potato starch nanoparticles. *Ultrasonics Sonochemistry, 51*, 444–450.

Soest, J. J. G.v., Tournois, H., Wit, D.d., & Vliegenthart, J. F. G. (1995). Short-range structure in (partially) crystalline potato starch determined with attenuated total reflectance Fourier-transform IR spectroscopy. *Carbohydrate Research, 279*, 204–214.

Sun, B., Di, H., Zhang, J., Xia, P., Huang, W., Jian, Y., et al. (2021). Effect of light on sensory quality, health-promoting phytochemicals and antioxidant capacity in post-harvest baby mustard. *Food Chemistry, 339*, Article 128057.

Tizzotti, M. J., Sweedman, M. C., Tang, D., Schaefer, C., & Gilbert, R. G. (2011). New ^{1}H NMR procedure for the characterization of native and modified food-grade starches. *Journal of Agricultural and Food Chemistry, 59*(13), 6913–6919.

Vilaplana, F., & Gilbert, R. G. (2010). Two-dimensional size/branch length distributions of a branched polymer. *Macromolecules, 43*(17), 7321–7329.

Villanueva-Flores, F., Castro-Lugo, A., Ramirez, O. T., & Palomares, L. A. (2020). Understanding cellular interactions with nanomaterials: Towards a rational design of medical nanodevices. *Nanotechnology, 31*(13), Article 132002.

Wang, K., Hasjim, J., Wu, A. C., Henry, R. J., & Gilbert, R. G. (2014). Variation in amylose fine structure of starches from different botanical sources. *Journal of Agricultural and Food Chemistry, 62*(19), 4443–4453.

Wang, J., Hu, P., Chen, Z., Liu, Q., & Wei, C. (2017). Progress in high-amylose cereal crops through inactivation of starch branching enzymes. *Frontiers in Plant Science, 8*, 469.

Wang, P., Lombi, E., Zhao, F. J., & Kopittke, P. M. (2016). Nanotechnology: A new opportunity in plant sciences. *Trends in Plant Science, 21*(8), 699–712.

Wang, S., Wang, S., Guo, P., Liu, L., & Wang, S. (2017). Multiscale structural changes of wheat and yam starches during cooking and their effect on in vitro enzymatic digestibility. *Journal of Agricultural and Food Chemistry, 65*(1), 156–166.

Wu, X., Chang, Y., Fu, Y., Ren, L., Tong, J., & Zhou, J. (2016). Effects of non-solvent and starch solution on formation of starch nanoparticles by nanoprecipitation. *Starch, 68*(3–4), 258–263.

Xing, J., Yan, F., Zhao, Y., Chen, S., Yu, H., Zhang, Q., et al. (2016). High-efficiency light-emitting diodes of organometal halide perovskite amorphous nanoparticles. *ACS Nano, 10*(7), 6623–6630.

Zhang, Q., Ying, Y., & Ping, J. (2022). Recent advances in plant nanoscience. *Advanced Science, 9*(2), Article 2103414.

Zhong, Y., Li, Z., Qu, J., Bertoft, E., Li, M., Zhu, F., et al. (2021). Relationship between molecular structure and lamellar and crystalline structure of rice starch. *Carbohydrate Polymers, 258*, Article 117616.